

Supplementary Material:

Evaluation of global EMEP MSC-W (rv4.34)-WRF (v3.9.1.1) model surface concentrations and wet deposition of reactive N and S with measurements

Yao Ge^{1,2}, Mathew R. Heal,¹ David S. Stevenson³, Peter Wind⁴, Massimo Vieno²

¹ School of Chemistry, University of Edinburgh, Joseph Black Building, David Brewster Road, Edinburgh, EH9 3FJ, UK

² UK Centre for Ecology & Hydrology, Bush Estate, Penicuik, Midlothian, EH26 0QB, UK

³ School of GeoSciences, University of Edinburgh, Crew Building, Alexander Crum Brown Road, Edinburgh, EH9 3FF, UK

⁴ The Norwegian Meteorological Institute, Henrik Mohns Plass 1, 0313, Oslo, Norway

Correspondence to: Yao Ge (Y.Ge-7@sms.ed.ac.uk), Mathew R. Heal (M.Heal@ed.ac.uk)

Model evaluation statistics

The unit of atmospheric concentration used in this work is $\mu\text{g m}^{-3}$. The ppb mixing ratios of gaseous species downloaded from some network websites were converted to mass concentrations via the ideal gas law ($pV = nRT$) and assuming 1 atmosphere pressure:

$$\mu\text{g m}^{-3} = \frac{\text{ppb} \times M}{0.0821 \times (273.15 + T)}$$

where T is the temperature in $^{\circ}\text{C}$, M is molecular mass of the gaseous pollutant (g mol^{-1}) and $0.0821 \text{ L atm K}^{-1} \text{ mol}^{-1}$ is the ideal gas constant R .

The following statistical metrics were calculated to compare model and observation data where M_i and O_i are modelled and observed (i.e. measured) data in a dataset of n such pairs. If a model grid contains more than one measurement site, the average of the measurements is used as O_i .

Pearson's correlation coefficient:

$$R = \frac{\sum_{i=1}^n (M_i - \bar{M})(O_i - \bar{O})}{\sqrt{\sum_{i=1}^n (M_i - \bar{M})^2} \sqrt{\sum_{i=1}^n (O_i - \bar{O})^2}}$$

Mean bias:

$$M_B = \frac{1}{n} \sum_{i=1}^n (M_i - O_i) = \bar{M} - \bar{O}$$

Mean absolute error:

$$M_E = \frac{1}{n} \sum_{i=1}^n |M_i - O_i|$$

Normalized mean bias:

$$NMB = \frac{\sum_{i=1}^n (M_i - O_i)}{\sum_{i=1}^n O_i} = \left(\frac{\bar{M}}{\bar{O}} - 1 \right)$$

Normalized mean error:

$$NME = \frac{\sum_{i=1}^n |M_i - O_i|}{\sum_{i=1}^n O_i} = \frac{M_E}{\bar{O}}$$

NO_x and SO_x emission differences between HTAP and ECLIPSEE inventories

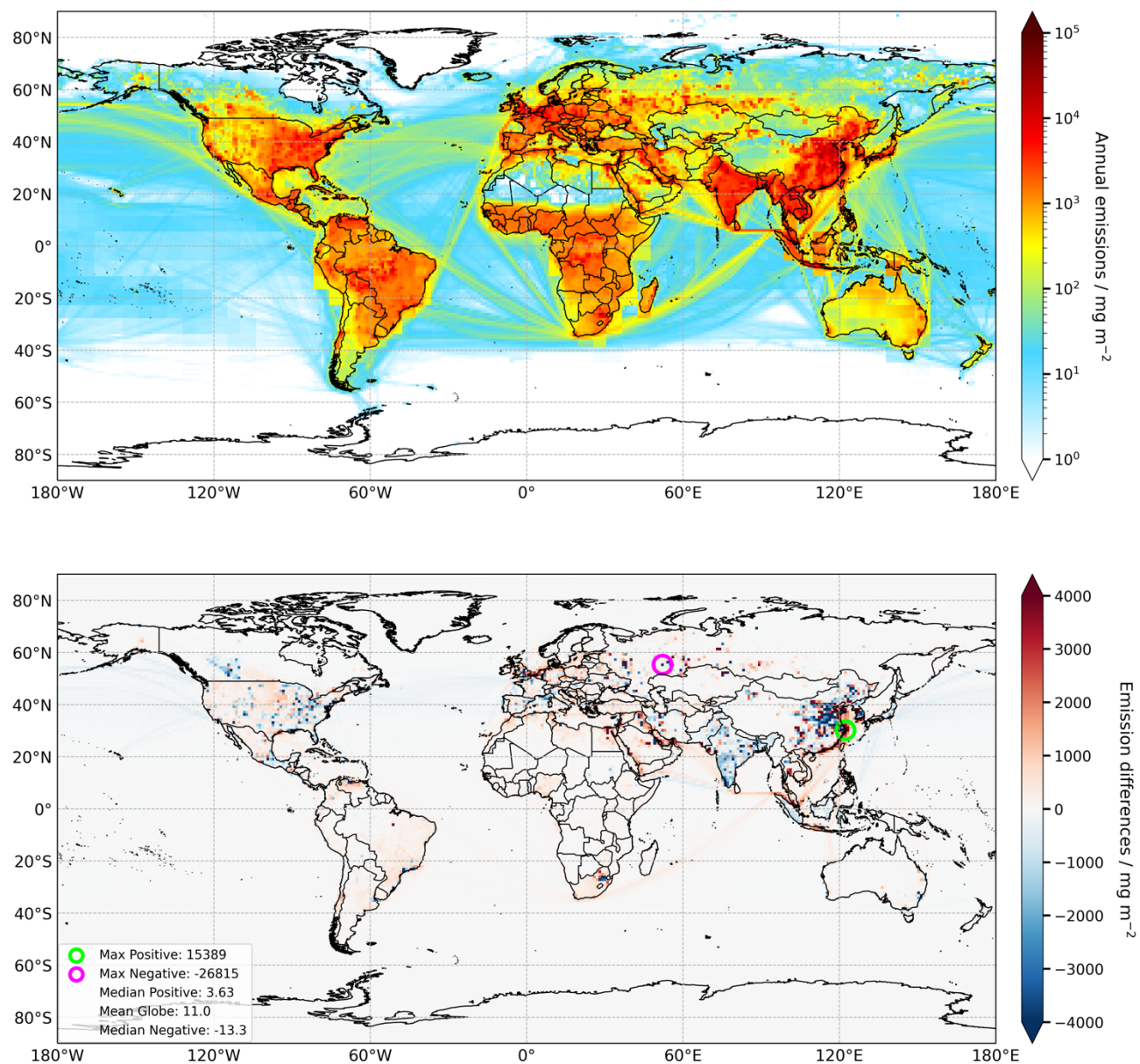


Figure S1. Top: Global annual NO_x emissions for 2010 from ECLIPSEE. Bottom: the difference in 2010 annual NO_x emissions (mg m⁻²) between ECLIPSEE and HTAP (ECLIPSEE – HTAP). The inset panel provides the maximum, median and mean values of both positive and negative differences across individual emission grids.

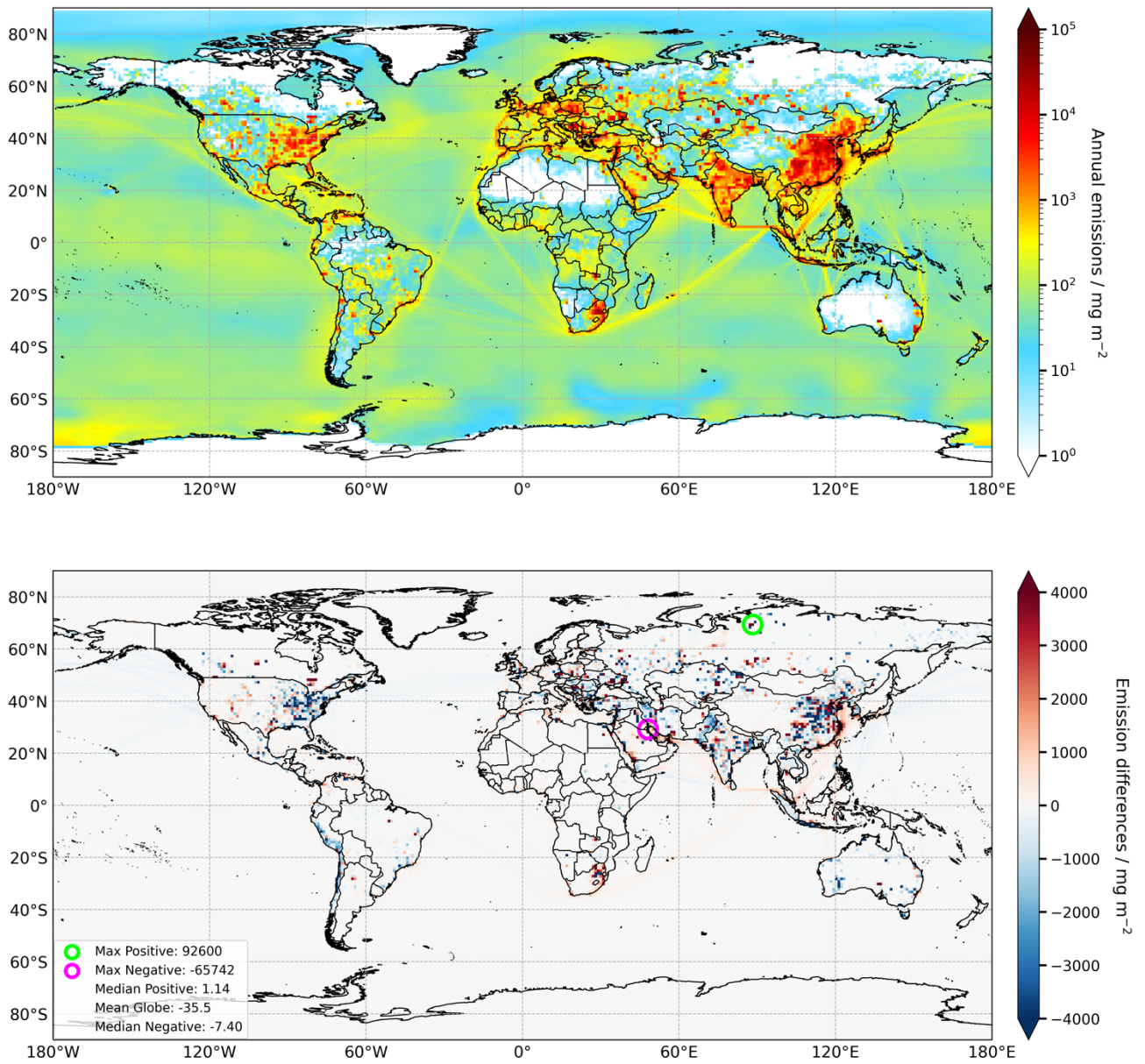


Figure S2. Top: Global annual SO_x emissions for 2010 from ECLIPSE_E. Bottom: the difference in 2010 annual SO_x emissions (mg m⁻²) between ECLIPSE_E and HTAP (ECLIPSE_E - HTAP). The inset panel provides the maximum, median and mean values of both positive and negative differences across individual emission grids.

Comparisons of monthly profiles of the HTAP and ECLIPSE_E emission inventories

Figure S3 presents a global map of annual terrestrial NH₃ emissions from ECLIPSE_E (i.e. ECLIPSE annual total emission with EDGAR monthly profile) in 2010. The boxes on the map delineate four example regions with measurement networks that are subsequently used to compare model and measurement concentrations spatially and seasonally, as reported in the main paper. Figure S4 compares the spatially-averaged monthly NH₃ emissions of the HTAP and ECLIPSE_E inventories in 2010 in each of these four global regions.

There is clear seasonality in NH₃ emissions in all four regions. In East Asia, the ECLIPSE_E inventory has larger NH₃ emissions than the HTAP inventory across all months and has a prominent maximum in spring, in addition to the general elevated emissions in summer projected by both inventories. For Southeast Asia, both the HTAP and ECLIPSE_E inventories present a distinct peak in NH₃ emissions in March, with the HTAP inventory having larger emissions than the ECLIPSE_E inventory in most months of the year, particularly in winter (as a consequence of smaller annual variation in the HTAP NH₃ emissions).

In Europe and North America there is generally good coincidence in magnitude and seasonality of NH₃ emissions between the two inventories. In Europe, both inventories project maximum NH₃ emissions in March and April, although the ECLIPSE_E inventory also projects a second maximum in August. The annual average emissions in Europe are similar, with sometimes one inventory and sometimes the other having higher emission in an individual month. In contrast, in North America, both inventories project maximum NH₃ emissions in July and August and much less pronounced peaks in early spring. In this region it is the HTAP inventory that projects the greatest annual variation, in contrast to East and Southeast Asia where ECLIPSE_E projects the greatest annual variation. The spring and summer peaks in NH₃ emissions in all four world regions reflect both agricultural activities (the dominant source of NH₃) and meteorological conditions. Larger NH₃ emissions in spring are associated with intensive manure and synthetic fertilizer application, whilst the rising temperatures throughout the summer favour the volatilisation of NH₃ from all sources.

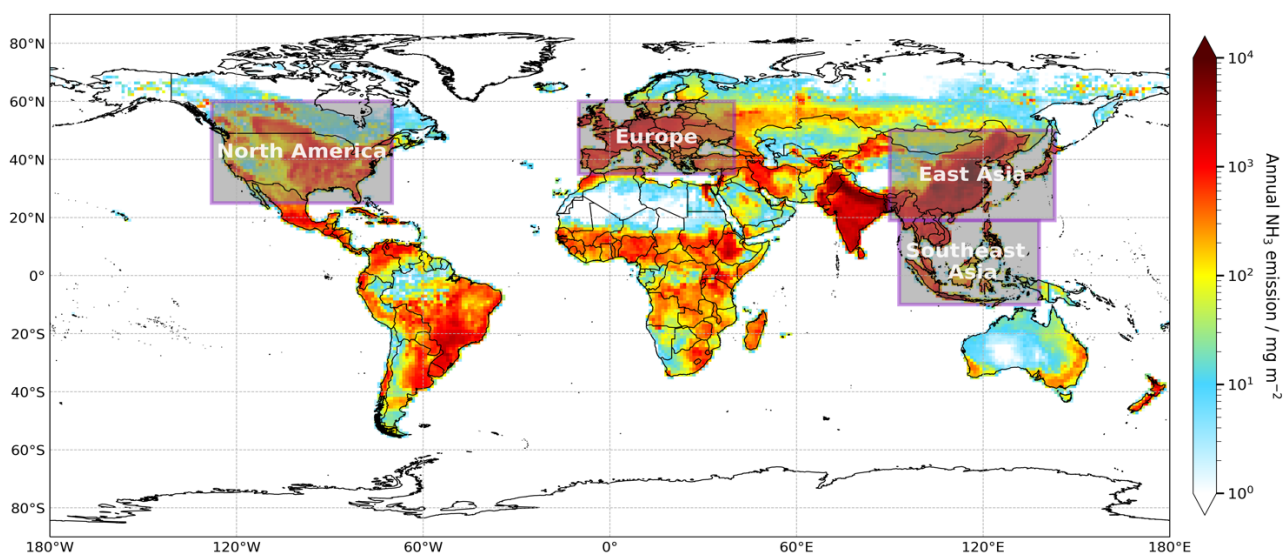


Figure S3. Global annual NH₃ emissions (mg m⁻²) for 2010 from the ECLIPSE_E inventory as implemented in the EMEP MSC-W model simulations in this work. The grey boxes show four regions in which monthly emission profiles of the ECLIPSE_E and HTAP inventories are compared.

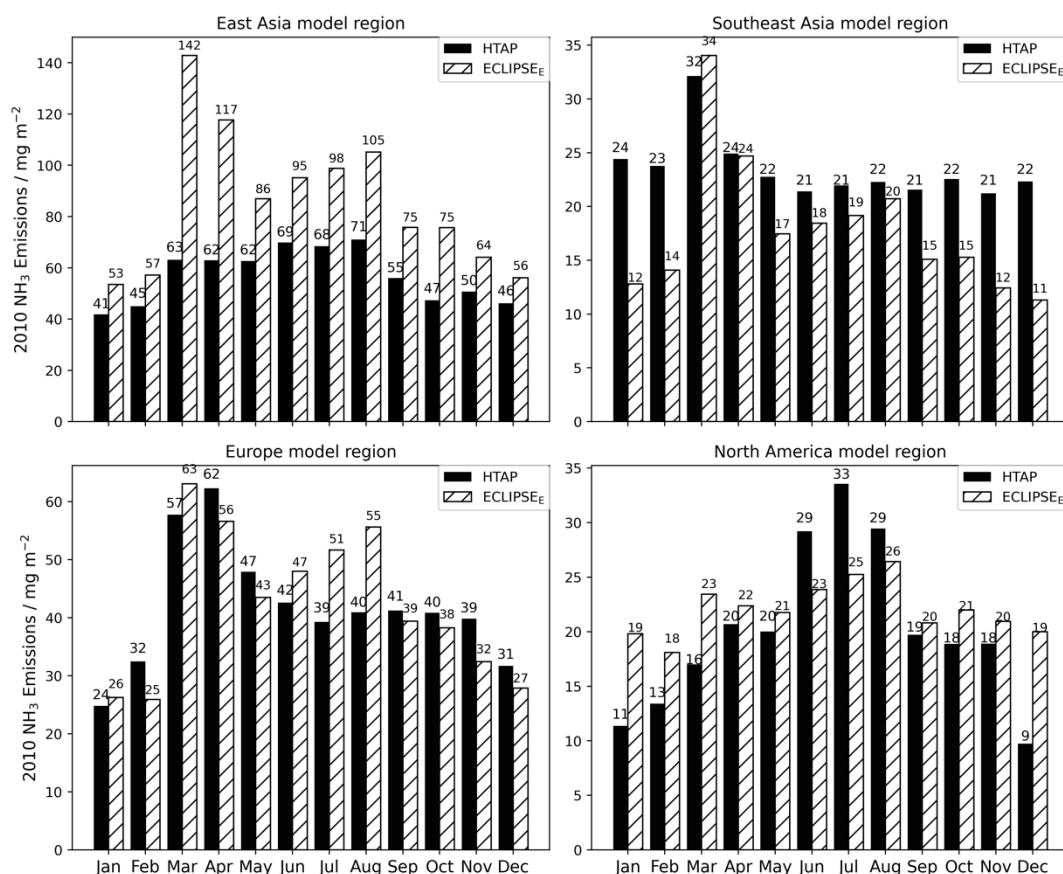


Figure S4. Monthly variations in the 2010 NH₃ emissions per unit area of the HTAP and ECLIPSE_E inventories averaged across each of the four model regions illustrated in Fig. S3: East Asia, Southeast Asia, Europe and North America. Note the different vertical scales in each panel.

Comparisons between use of HTAP and ECLIPSE_E emission inventories: NH₄⁺ concentration

The influences of the two emission inventories on model simulated surface concentration differs according to consideration of primary or secondary component and varies from one region to another. In general, concentrations of primary pollutants are more influenced by the local emissions, while secondary species are much less so. Fig. S5 compares the modelled NH₄⁺ concentrations using the two emission inventories for the grids in which there are also available measurements from the monitoring networks.

The differences in NH₄⁺ concentrations in simulations using the two emission inventories are smaller than for NH₃ (Fig. 4), as shown by concentrations that are closer to 1:1 in all regions. For example, whilst modelled NH₃ concentrations in China derived using the ECLIPSE_E inventory are on average 56% higher than those derived using the HTAP inventory, the NH₄⁺ concentrations are very similar. The annual average NH₄⁺ concentrations (based on network locations) in China are 7.30 and 7.15 μg m⁻³ for HTAP and ECLIPSE_E respectively, which is a difference of only 2%. The regression equation of NH₄⁺ concentrations from the model simulations with the two inventories across the full set of measurement network locations considered in this work is excellent ($y = 0.92x + 0.01$, $R = 0.98$, Fig. S5). This indicates good global consistency for the WRF-EMEP modelling system across a wide variation of primary NH₃, NO₂ and SO₂ emissions in different global

regions. It can be noted, however, that model simulations with both HTAP and ECLIPSE_E inventories yield slightly higher concentrations than measurements at lower concentrations (below 5 $\mu\text{g m}^{-3}$) but lower concentrations than measurements at higher concentration ranges. This reflects a fundamental difference between modelled and measured data. The modelled value represents the average concentration over a grid of several 10s km in horizontal dimension, whereas the measured values only represent the concentration at the specific location of the measurement. Since the latter are readily impacted by local sources and sinks, they will generally have a greater range in values which are averaged out in the former. Measurements are also sometimes deliberately sited in locations of anticipated high pollutant concentration that may be reduced by grid averaging in relatively spatially coarse global model simulations.

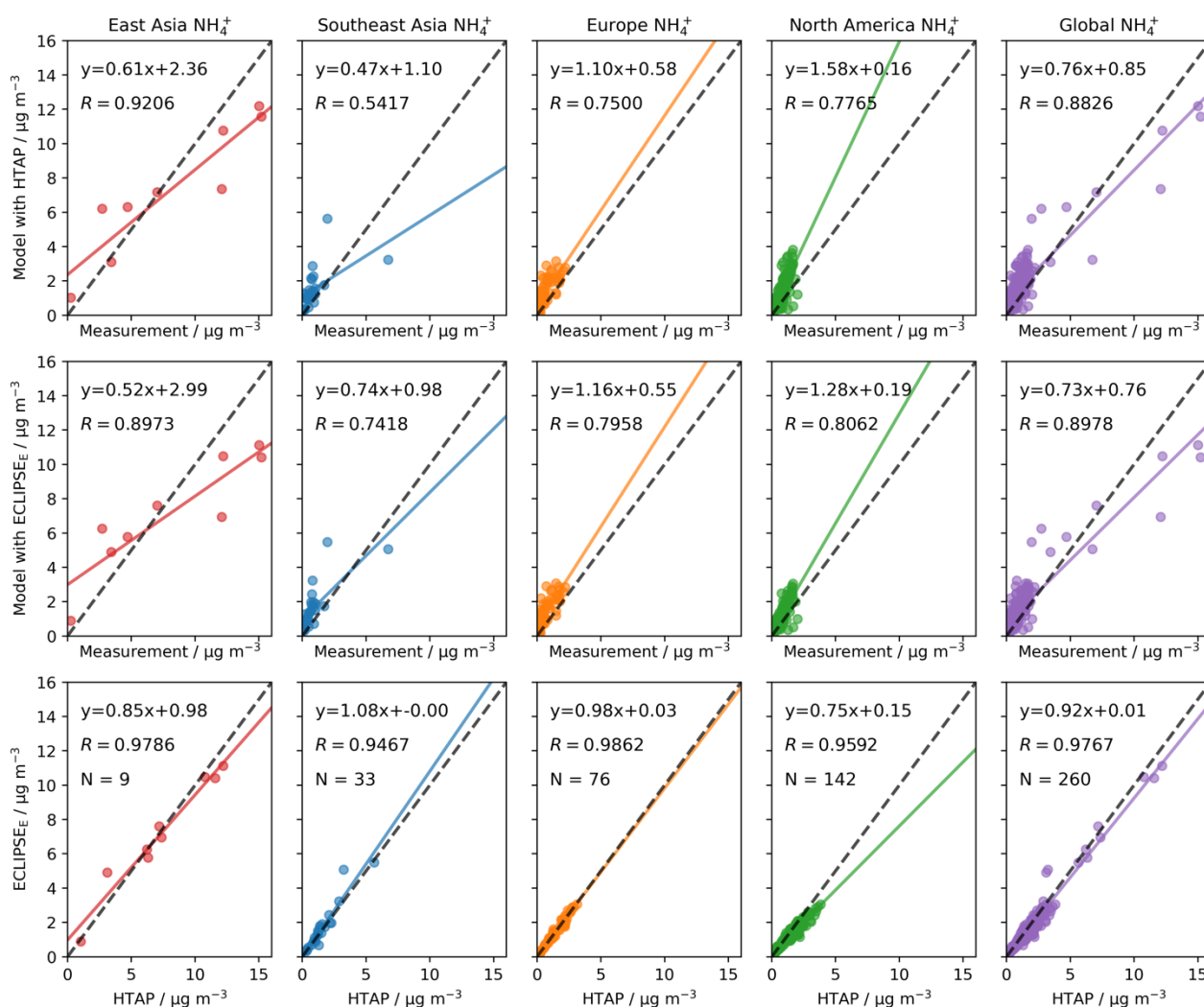


Figure S5. Comparisons of annual average surface concentrations of NH_4^+ for 8 monitoring networks in 2010 – NNDMN from China as East Asia, EANET as Southeast Asia, NAMN and AGANet (UK) and EMEP/CCC plotted together here as Europe, and the EPA and AMoN (USA) and NAPS (Canada) plotted together here as North America – and for all networks combined ('global'). The upper row of plots is modelled versus measured using the HTAP emission inventory. The middle row is modelled versus measured using the ECLIPSE_E emission inventory. The lower row is the modelled data for the two inventories plotted against each other for the same set of model grids that contain measurement sites. In each plot, N is the total number of scatter points, R is the Pearson correlation coefficient, the black dashed line is the 1:1 line and the coloured solid line is the trend line corresponding to the equation presented.

Comparison of temporal variation of modelled NH_4^+ concentrations with measurements

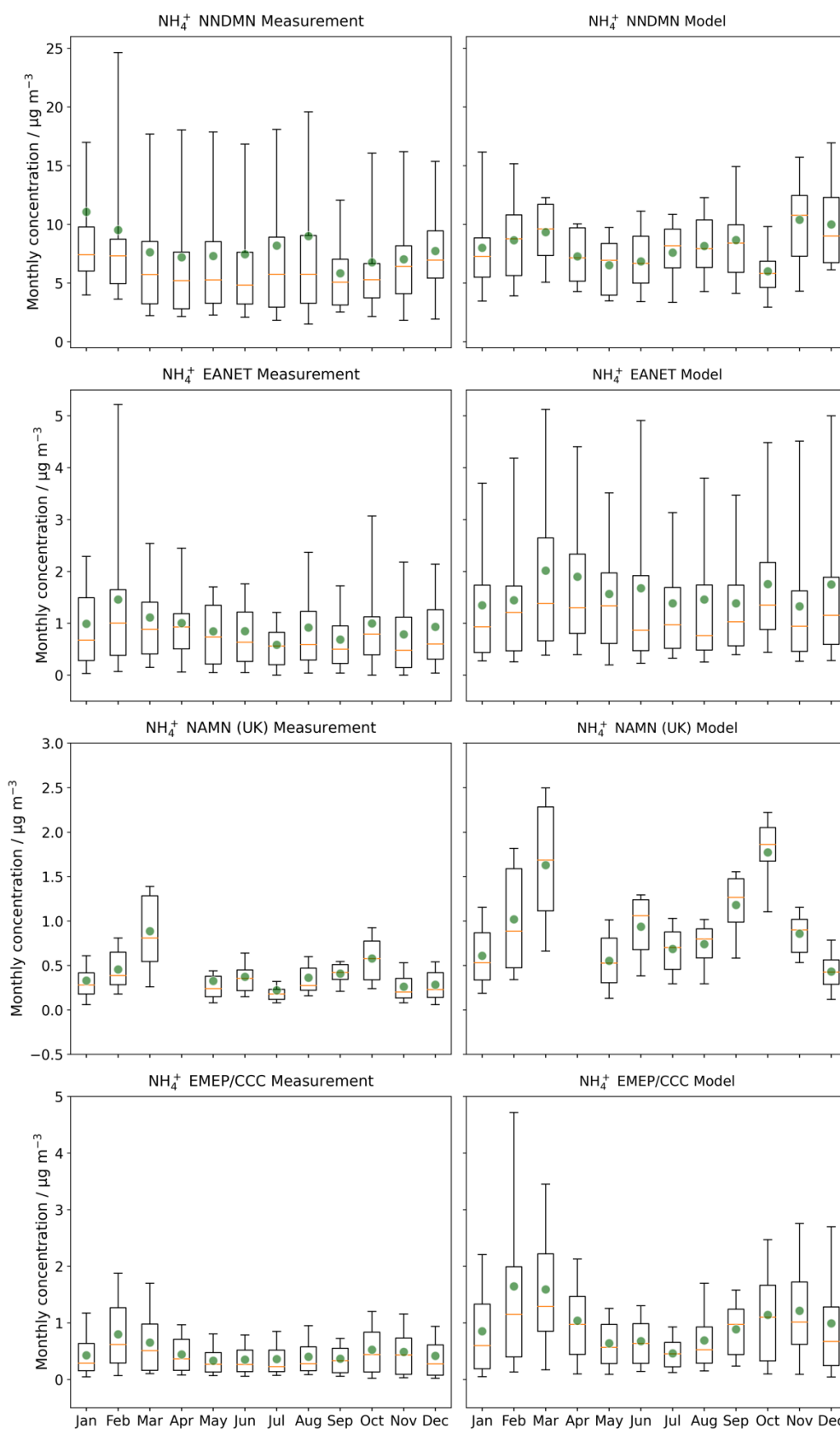


Figure S6. Monthly averaged measured (left panels) and modelled (right panels) NH_4^+ concentrations in 2015 for NNDMN, EANET, AGANet (UK) and EMEP/CCC monitoring networks. The box extends from the lower to upper quartile values of the data, with an orange line at the median and a green point at the mean. The whiskers represent 5% and 95% percentiles.

Comparison of modelled precipitation and wet deposition with measurements

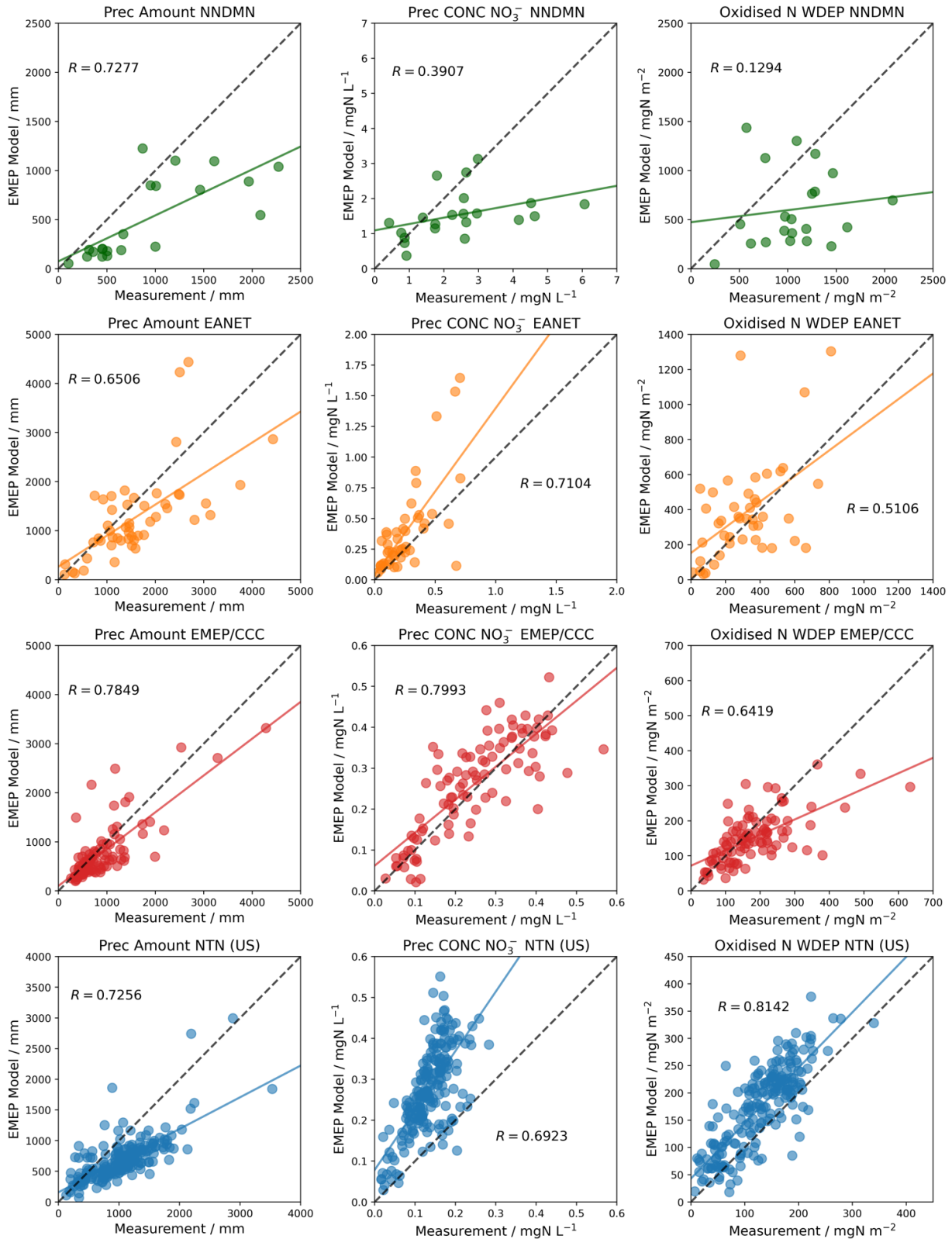


Figure S7. Scatter plots of model-measurement comparisons of 2015 annual wet deposition variables for oxidized N (as NO_3^-) for four measurement networks: NNDMN, EANET, EMEP/CCC and US NTN. Left panels are annual precipitation. Middle panels are precipitation-weighted annual average NO_3^- concentration in precipitation. Right panels are annual total wet deposition of NO_3^- . In each plot, the coloured line is the least squares regression and the black dashed line is the 1:1 line.

Table S1. Summary statistics of model comparison with measurements (referred to here as ‘O’ for observation) for annual precipitation amount (Prec Amount, mm), precipitation-weighted annual mean concentration of NO₃⁻ (Prec Conc, mgN L⁻¹), and wet deposition of oxidized N (WDEP, mgN m⁻²) for four measurement networks in 2015. *N* is the number of measurement sites. *R* is Pearson’s coefficient. Fac2 fraction is the proportion of data points that are within a factor of 2. Mean_O and Mean_M of Prec Conc are annual averages of observation and model respectively. Mean_O and Mean_M of Prec Amount and WDEP are annual totals. NMB is normalized mean bias, NME is normalized mean error.

| Networks | Variables | <i>N</i> | <i>R</i> | Fac2 fraction | Mean_O | Mean_M | NMB | NME |
|---------------|-------------|----------|----------|---------------|--------|--------|-------|------|
| China | Prec Amount | 21 | 0.73 | 0.43 | 913 | 502 | -0.45 | 0.49 |
| | Prec Conc | 21 | 0.39 | 0.67 | 2.43 | 1.54 | -0.37 | 0.46 |
| | WDEP | 21 | 0.13 | 0.38 | 1068 | 605 | -0.43 | 0.56 |
| East Asia | Prec Amount | 50 | 0.65 | 0.82 | 1585 | 1270 | -0.20 | 0.39 |
| | Prec Conc | 46 | 0.71 | 0.59 | 0.26 | 0.39 | 0.52 | 0.71 |
| | WDEP | 44 | 0.51 | 0.68 | 316 | 384 | 0.22 | 0.56 |
| Europe | Prec Amount | 101 | 0.78 | 0.91 | 863 | 749 | -0.13 | 0.31 |
| | Prec Conc | 93 | 0.80 | 0.92 | 0.24 | 0.26 | 0.06 | 0.24 |
| | WDEP | 93 | 0.64 | 0.90 | 179 | 151 | -0.16 | 0.32 |
| United States | Prec Amount | 206 | 0.73 | 0.82 | 1030 | 690 | -0.33 | 0.39 |
| | Prec Conc | 207 | 0.69 | 0.41 | 0.13 | 0.27 | 1.04 | 1.05 |
| | WDEP | 206 | 0.81 | 0.87 | 129 | 174 | 0.35 | 0.41 |